Author's Accepted Manuscript

The effect of wheel eccentricity and run-out on grinding forces, waviness, wheel wear and chatter

Jeffrey Badger, Stuart Murphy, Garret O'Donnell

www.elsevier.com/locate/ijmactool

Cite this article as: Jeffrey Badger, Stuart Murphy and Garret O'Donnell, The effect of wheel eccentricity and run-out on grinding forces, waviness, wheel wear and chatter, *International Journal of Machine Tools & Manufacture*, doi:10.1016/j.ijmachtools.2011.06.006

The effect of wheel eccentricity and run-out on grinding forces, waviness, wheel wear and chatter

Jeffrey Badger[1], Stuart Murphy[2], Garret O'Donnell[2]

[1]*The Grinding Doc*, Austin, Texas, USA

[2]Trinity College, Dublin, Ireland

VITAE

Jeffrey A. Badger, Ph.D. is an expert in grinding. He works independently as "The Grinding Doc", a consultant in grinding. He continues to do research in the field and has strong ties to Trinity College, Dublin, where he did his Ph.D. and is currently an adjunct professor. His is widely published in the academic journals and in CIRP. Contact: +1-512-934-1857 // JB@TheGrindingDoc.com // 31415 Falling Shadows Drive; Bulverde, TX 78163.

Dr. Garret O Donnell is a University lecturer in the Department of Mechanical and Manufacturing Engineering in Trinity College Dublin and a research affiliate member of CIRP. Garret's research activity in Trinity College Dublin is based on advancing manufacturing technologies that underpin sectors such as biomedical, automotive, aerospace, and ICT. His principal research area is the process monitoring of machining processes with goals of understanding the fundamental science, developing new sensor concepts, signal processing algorithms, intelligent decision making strategies and adaptronic control systems for high performance cutting processes. Contact: ODONNEGE@tcd.ie.

Stuart Murphy is a Ph.D. candidate at Trinity College. His research areas are in grinding are in eccentricity, loading, process monitoring via acoustic emission and force measurements. His current project is determining dressing-wear characteristics in CVD and natural diamonds. Contact: murphs12@tcd.ie.

The effect of wheel eccentricity and run-out on grinding forces, waviness, wheel wear and chatter

Abstract

The effect of grinding-wheel eccentricity on grinding forces, wheel wear and final waviness height was studied. Eccentricity was evident in force oscillations and acceleration and audio measurements. A model was developed to predict final scallop-profile shape from grinding parameters and eccentricity. Recommendations are given on detecting eccentricity and determining when eccentricity is tolerable.

Keywords: eccentricity, run-out, scallop, chatter, waviness, truth

1 INTRODUCTION

A grinding wheel rotating about a central axis, O, as shown in Figure 1, will not be perfectly true. It will be: a) an imperfect, non-circular shape, R=f(θ)$\neq$constant; b) a perfect circle, R=constant, centered around the axis O' , a distance ε from O; or c) some combination of the two. In fact, no wheel is perfectly true or concentric, and the degree of untruth will have a profound effect on the grinding performance.

In Al_2O_3, SiC, and most CBN wheels, the wheel is dressed true prior to grinding. Therefore, any untruth or eccentricity is "dressed away". In some CBN wheels and most bonded diamond wheels, the wheel is trued "off machine" on a separate truing station and returned to the grinding machine, where eccentricity is introduced when the wheel is remounted. Dirt can also introduce run-out, as high as 130 μm [1].

The standard safety code requires that all wheels are manufactured with a bore diameter larger than the shaft diameter to allow for the expansion due to heat and centrifugal forces [2]. When the wheel is remounted on the non-tapered spindle, run-out will depend on the tolerances in the wheel and spindle. Most superabrasive wheels are manufactured to a bore-diameter tolerance of H7 or H6. A 37.5-mm bore has an H7 tolerance of +0/-0.025 mm, an H6 of +0/-0.016 mm. Therefore, run-out can be high.

Bennet and May [3] analyzed the effect of eccentricity and imbalance in centerless grinding and found that the wheel can shift on the hub due to grinding forces. Arizmendi *et. al.* [4] predicted surface topography from eccentricity in milling. Inasaki discussed the effect of run-out on chatter as a function of material-removal rate, along with an optical sensor to measure run-out [5]. Armarego and Deshpande predicted force and torque values in due to eccentricity in end-milling [6]. Trmal and Holesovsky [7] showed how wave shift can affect waviness on cylindrically ground parts. A similar situation was found by Rowe and Barash in centerless grinding [8]. Rowe found a series of scallops on the workpiece with the scallop height being a function of chatter wavelength and wheel diameter [9]. Rowe also discussed how a long arc-length and a short chatter wavelength both facilitate attenuation [9]. Several Japanese researchers explored obliterating waviness caused by chatter by shifting the phase shift [5].

In spite of this, little has been written on how grinding-wheel untruth affects forces, wheel wear and temperatures, on processing monitoring to detect untruth, and how the waviness scallop shape develops based on the grinding parameters. This paper attempts to rectify that situation.

Figure 1. Untruth and eccentricity in grinding wheel.

2 THOERY AND CALCULATIONS

The chatter wavelength, ℓ_{wv}, is the distance the workpiece moves during one vibration, can be calculated by ℓ_{wv}=v_w/f, where v_w is the feedrate in mm/s and f is the vibration frequency in Hz. For self-excited chatter, this frequency is typically around the natural frequency of the wheel/workpiece system; for forced chatter, it is the frequency of the vibration source. For wheel untruth with a single high point on the wheel, it is the wheel rotational speed.

If we take a single point on the wheel, then that point will trace out a path which leaves a series of scallops on the wheel with a height, h_{sc}, of:

$$h_{sc} = \frac{\ell_{wv}^2}{4 \cdot d_s} \qquad (1)$$

If the arc length, ℓ_c, is sufficiently long, the height of the scallop will be attenuated. This threshold is [9]

$$\ell_c > \ell_{wv}/2 \qquad (2)$$

However, this assumes a single-point on the wheel, more like a milling cutter. A grinding wheel has a multitude of small cutting points around the perimeter.

2.1 *Continuous Scalloping*

Instead, we can take the radius as function of the angle, θ. If the untruth about the central axis is an eccentricity in the wheel, then the radius of the wheel from the central axis will be:

$$R_\theta = \frac{d_s}{2} + \varepsilon \cdot \cos(\theta) \qquad (3)$$

Since the outermost point of the grinding wheel will trace out a motion path as shown in Figure 1, we can calculate, h_θ, the distance from the bottommost point to the contact point of the grinding wheel, by:

$$h_\theta = \varepsilon - \varepsilon \cdot \cos(\theta) \qquad (4)$$

The "scallop effect" will occur not just when the wheel is at its bottommost point but, in fact, in all situations regardless of part dimensions and parameters. This is because the slope at the bottommost portion of the wheel will be 0 (i.e., "horizontal"), as shown in Figure 2.

Only under specific situations, however, will it act to reduce the maximum scallop height, namely with an arc length that extends beyond the highest point in the wave (a). In other situations, it will scallop only along the edges of the profile but will not reduce the maximum scallop height (b).

If we take a point A at a distance x', as shown in Figure 3, the scallop arc length, $l_{c,sc}$, required to hit the highest point will vary along the curve.

If we assume a bottommost point of the wheel lies at some point A along the run-out curve, substituting in θ = x ·2π/l_{wv}, and x=x' into Eq. 1, we obtain,

Figure 2. Scallop effect for different arc lengths.

Figure 3. Continuous scalloping effect.

$$y1 = \varepsilon - \varepsilon \cdot \cos(x' \cdot 2\pi/l_{wv}) \qquad (5)$$

The arc length, $l_{c,sc}$, is calculated by [10]

$$l_c = \sqrt{a_e d_e} \qquad (6)$$

where a_e=y2 and l_c =$l_{c,sc}$=x2. We can now take

$$x1 + x2 = l_{wv}/2 \qquad (7)$$

and

$$y1 + y2 = 2\varepsilon \qquad (8)$$

We can then solve for de to obtain:

$$d_e = \frac{\left(\dfrac{\ell_{wv}}{2} - x'\right)^2}{\varepsilon + \varepsilon \cdot \cos\left[\dfrac{2 \cdot \pi}{\ell_{wv}} x'\right]} \qquad (9)$$

Now we have, at any given point x', the required wheel diameter to truncate the scallop. If we substitute in x'=0 and 2ε=h_{sc}, we obtain Eq. 1.

Now that we have determined the criteria for when the scallop effect reduces the scallop height, we can determine the actual scallop shape.

2.2 *Scallop-waviness model*

If we take the centerline position of the wheel at point A, at x=x1=x' and y=y1, and trace out the arc of the current position of the grinding wheel, we obtain a y3=f(x) as shown in Figure 4. This is the instantaneous shape imparted into the workpiece by the wheel when the wheel is at the centerline position x'. The distance x3 is then:

$$x3 = x - x' \qquad (10)$$

Figure 4. Wheel profile at given point x'.

The path carved out by the wheel will simply follow the equation of a circle ($x^2+y^2=R^2$) with the origin at x'. Therefore, the height y3 can be calculated by:

$$y3 = \frac{d_e}{2} - \sqrt{\left(\frac{d_e}{2}\right)^2 - (x-x')^2} \qquad (11)$$

so the wheel profile, y_s =y1+y3, will follow the curve

$$y_s = \varepsilon - \varepsilon \cdot \cos(x' \cdot 2\pi/\ell_{wv}) + \frac{d_e}{2} - \sqrt{\left(\frac{d_e}{2}\right)^2 - (x-x')^2} \quad (12)$$

and the height at any point x will be:

$$y(x) = \text{minimum} [\, y1(x), y_s(x)\,] \qquad (13)$$

These concepts were implemented into the *Scallop Waviness Model*, which predicts final profile shape and scallop height from the grinding parameters and wheel eccentricity.

2.3. Waveshift

Most grinding operations take repeated depths of cut, often at depths smaller than the previously imparted scallop height and smaller than the run-out in the wheel, and with one or several spark-out passes at zero depth of cut where the waves may be shifted relative to the previous wave. Therefore, the model was developed to superimpose into the workpiece successive passes, including spark-out passes (a_e=0), each with a specified wave-shift, ℓ_{sh}.

In cylindrical grinding, this wave shaft can be calculated by the ratio of wheel rotational speed to workpiece rotational speed [3, 5]. In surface grinding, however, this wave shift will be more or less random.

3 MATERIAL AND METHODS

Tests were done on a Jones & Shipman 540 surface grinder using a white-alumina, 60-mesh, K-grade, vitrified-bonded grinding wheel (d_s=200 mm, ω=2880 RPM, v_s=30.1 m/s) grinding either a) D2 tool steel (30 Rc, ℓ=65 mm, w=10 mm) or b) 304L stainless steel (workpiece length and width: l_{wp}=100 mm, b_{wp} =2 mm) with various depths of cut and feedrates (a_e=2 μm, 4 μm, 6 μm, 10 μm, 20 μm and 40 μm; v_w=36 to 307 mm/s) after dressing with a single-point dressing diamond (a_d=0.002 mm, s_d=0.3 mm, 5 passes, 1 finishing pass). Normal and tangential forces were measured with a Kistler, 3-axis piezoelectric dynamometer (10 kHz). Wheel run-out was measured with a dial gauge (d_{ball}=2.5 mm) every 5º (72 points). In some tests, wheel eccentricity was created after dressing by dismounting and remounting the wheel on the flange, rebalancing and remounting on the machine spindle. Wheel wear was measured by the "razor-blade test" [10] at depths of 0.5, 1.0, 2.0, 3.0, 4.0, 5.0 and 6.0 mm. The wheel wear was calculated as volume of material removed per mm wheel width per mm wheel circumference by:

$$V_w'' = \frac{a_e \cdot \ell_{wp} \cdot b_{wp} / b_{wp}}{\pi \cdot d_s} = \frac{a_e \cdot \ell_{wp}}{\pi \cdot d_s} \qquad (14)$$

The wheel-wear depth was normalized as a fraction of the grit diameter [10] (60-mesh: d_{grit}=253 μm).

Profiles of the workpiece were taken with a Hommel profilometer after grinding, with a spacing of 0.004 mm/sample in the direction of the grind. A 3-D profile of the surface was also taken using an Omniscan MicroXam white-light interferometer. Acceleration was measured with a piezoelectric accelerometer (500 mV/g) which was magnetically mounted on top of the spindle 20 mm from the rear of the wheel, sampling at 4000 Hz.

An audio signal was recorded with an industrial microphone mounted 20 mm from the center of the workpiece, sampling at 44,100 Hz.

4 RESULTS

4.1 *Run-out measurement results*

Figure 5 shows the run-out measured by the dial gauge for the wheel: 1) after dressing; 2) after eccentricity was added; and 3) after grinding. Measured run-out values were 1) RO=14 μm, 2) RO=95 μm, and 3) RO=38 μm.

In fact, if we consider the diameter of the ball in the dial gauge and assume the width of a pore in the grinding wheel is of the same order as the grit diameter, a dial-gauge ball contacting on two outer grits and centered over a pore will give a displacement of h=14 μm $[(d_{ball}-h)^2+(d_{grit}/2)^2=d^2_{ball}]$. This is the same as the measured run-out value of the dressed wheel, indicating that the actual run-out taken from the grain tips is closer to RO=2ε=0 μm.

Considering this, we can assume that actual run-out is 14 microns less than measured run-out, obtaining the following values:

1. RO=2e~0 μm   "near-true wheel"
2. RO=2e~81 μm   "highly eccentric wheel"
3. RO=2e~24 μm   "eccentric wheel"

Figure 5. Measured run-out values.

From the figure we can also see that run-out was reduced drastically after just a few tests (Test 2 to Test 3). This could be caused by two phenomena: 1) the wheel is shifting on the hub, as proposed by Bennett and May [3]; or 2) the wheel wear on the high point of the wheel is reducing eccentricity.

If wheel wear is the dominant reason, the grits on the high point would have worn about one-quarter of a grit diameter, which seems large considering the small amount of material removed. However, as will be shown next, forces in an eccentric wheel are much higher, which would accelerate wear on the high points.

On the other hand, if the wheel had simply shifted on the hub, we would expect the same half-sine-wave shape, but with a smaller amplitude throughout. This is not what we see in Figure 5; we see the original half sine-wave rising on either side, but truncated in the middle, at the high point. This indicates that wheel wear is, in fact, the dominant mechanism.

4.2 *Grinding Forces.*

Figure 6 shows the normal and tangential forces when grinding with a highly eccentric wheel (RO=2ε~81 μm) and a near-true wheel (RO=2ε~0 μm).

For the highly eccentric wheel, we see periods of wheel/workpiece contact and non-contact (contact time=37%, non-contact time=63%). Here the run-out (RO=2ε~81 μm) is higher than the grinding depth of cut (a_e=4 μm).

During the non-contact period, the workpiece is still moving laterally. Then, as the high point of the wheel comes about, it encounters an excess of material to remove, resulting in an increase in material-removal rate and a surge in forces.

In the situation with near-zero run-out, we see that grinding forces are much lower. We also see that contact never drops to zero.

Figure 7 shows the same grinding scenario as above, but with the depth of cut increased from a_e=4 μm to a_e=20 μm. Again, the highly eccentric wheel is causing surges in grinding forces while the near-true wheel gives steady forces. However, the non-contact region has decreased nearly to zero, although the increase in force relative to the near-true wheel was consistent at around 130%.

Figure 6. Grinding forces, a_e=4 μm.

Figure 7. Grinding forces, a_e=20 μm.

If we take an average of the near-true forces (Δt=0.003 s = 30 points=1/7 wheel revolution), we see a muted waviness corresponding to the wheel frequency – which is more evident in the a_e=20 μm case – indicating that either an imbalance or a slight eccentricity is present in the near-true wheel.

Although not shown here, when the depth of cut was kept at a_e=20 μm but the feedrate was decreased to 37 mm/s, no variation in average force was visible in the near-true wheel. The wavelength – which decreased from l_{wv}=6.4 mm to l_{wv}=0.7 mm – was shorter than the arc length of l_c=2.0 mm, resulting in wavelength attenuation – i.e., scalloping – at all values of x' and a perturbation of any tendency toward chatter.

4.3 *Self-excited chatter*

If we zoom in on the area shown in Figure 7, a period of about one-third of a wheel revolution, we see a secondary frequency of around 652 Hz, as shown in Figure 10. Jones & Shipman claim the natural frequency of a 540 machine is 650 Hz [11], indicating self-excited chatter. The peak-to-valley amplitude of normal force is around 4 N/mm, which corresponds to the maximum variation also shown in Figure 7. This indicates that the oscillation of forces may also occur at the wheel speed, but the excitation of this oscillation is self-excited rather than forced.

It is interesting to note that self-excited chatter was also visible in the force profiles of the highly eccentric wheel in the form of one or two "blips" at a frequency of around 650 Hz, in spite of that fact that this excitation did not have ample time for any regenerative effect to take place, as is typical [5].

Figure 8: Grinding forces in near-true wheel.

4.4 *Visual evidence*

Figure 9 shows the oxidation burn present on the ground surface after grinding with the highly eccentric wheel. Typically, for a true wheel, any oxidation burn that occurs in grinding is ground away. In the case of the untrue wheel, however, the periods of non-contact mean that patches of oxidation occur. Since oxidation burn occurs begins to occur at low temperatures, this does not indicate that genuine thermal damage occurred, just that the oxidation burn was not ground away.

From the figure we can see that "oxidation chatter marks" occur at one wheel revolution (l_{wv}=v_w/f=6.4 mm). We also see some additional burn marks occurring not quite half-way between the other chatter marks, indicating a phase shift of around l_{sh}=0.4·l_{wv}.

Photos were also taken after grinding with the slow feedrate (v_w=37 mm/s) with the highly eccentric wheel, giving a wavelength smaller than the arc length. Visual inspection of this workpiece showed only very slight oxidation burn marks, spaced much closer together, corresponding to the wheel frequency. Although the run-out was greater than the depth of cut, meaning times with no contact, the wavelength was small enough – l_{wv}=0.76 mm, l_c=0.90, 0.024 mm<RO<0.081 mm – to ensure "scalloping away" of the oxidation burn.

Figure 9: Oxidation burn from highly eccentric wheel.

4.5 *Scallop Results*

Figure 10 shows a 3-D map of the ground surface via white-light interferometry after grinding with the eccentric wheel (a_e=0.004 mm, v_w=281 mm/s). Here we can see that, although the arc length is much shorter than the wavelength (l_c=0.9 mm, l_{wv}=5.85 mm/rev), scalloping does occur and the criterion for maximum scallop height reduction (Eq. 9), was met. However, the height of the scallops is high – much higher than the depth of cut – indicating that multiple passes are creating the scallop height greater than the depth of cut.

Figure 10. Scallop shape on workpiece.

4.6 *Acceleration*

Figure 11 shows the Fourier transform of the acceleration-vs.-time signal for the grinding wheel during idling and during grinding (a_e=20 μm, v_w=307 mm/s) for a balanced yet eccentric wheel (RO=40 μm).

During wheel idling we see a series of high peaks in the 1200 to 1600 Hz region, which may correspond to bearing issues on the older machine. Around the wheel speed we see one small peak at the wheel speed of 0.001Gs. Converting this to displacement gives a amplitude of 0.2 μm, typical for a balanced wheel. During grinding, we still see the same peaks at the high frequencies. However, at lower frequencies, particularly at wheel speed and twice wheel speed, we see much larger peaks caused by grinding with the eccentric wheel.

Figure 11. FFT of acceleration signal.

4.7 *Audio*

A microphone placed near the workpiece gave a clear audible "tack tack tack" sound when grinding at the wheel speed. The decibel-vs.-time output is given in Figure 14. A wheel-frequency signal is evident during wheel idling, which increases drastically during grinding. An FFT of the signal during grinding gave peaks at 1X, 2X and 3X the wheel frequency.

Figure 12. Audio output signal.

4.8 *Wheel wear*

Additional tests were done on 304L stainless steel (a_e=4 μm, v_w=260 mm/s), grinding 6 mm depth of material with both a near-true wheel and a highly eccentric wheel and periodically measuring wheel wear with the "razor blade technique" [10]. The wear depth is given as a fraction of the grit diameter. A large amount of material was ground so that the wear depth was much greater than the initial wheel run-out (RO_i).

Figure 13: Wheel wear.

Results are given in Figure 13. We can see that wheel wear was about 60% higher for the highly eccentric wheel. We can also see that wheel wear was quite steady throughout. Considering this, along with the high aggressiveness [12] (Aggr=39) and low G-ratios, it appears that bond fracture is the dominant wear mechanism. It would be expected that the difference between G-ratios would be greater under less-aggressive grinding conditions, as is typical when attritious wear and grit fracture become more dominant [13].

4.9 *Specific Energy*

Figure 14 shows the specific energy, $e=P/Q$, calculated from the grinding power, P, and the material-removal rate, Q, vs. the Aggressiveness [12], Aggr, for the near-true, eccentric and highly eccentric wheels, with Aggressiveness calculated from:

$$Aggr = 1,000,000 \frac{v_w}{v_s} \sqrt{\frac{a_e}{d_e}} \qquad (15)$$

Figure 14: Specific energy.

As is typical, specific energy decreases with increasing Aggressiveness. We also see much higher values of specific energy for the highly eccentric wheel, rising by a factor of 5, to over 400 J/mm^3.

The calculation here assumes a constant material-removal rate (MRR). In fact, the MRR will rise and fall with the eccentric wheel. However, if we assume that during these power surges the maximum arc length, l, stays consistent with the standard l_c=$(a_e \cdot d_e)^{1/2}$ (Eq. 6), and if we assume a standard Jaeger model [14] where temperature is proportional to heat flux and, therefore for a fixed partition ratio, grinding power, we see that the eccentric wheel will give much higher surface temperatures.

5 DISCUSSION

5.1 *Scallop Waviness Model*

In Figure 10, we see a peak-to-valley scallop height of h_{sc}=0.024 mm and 0.018 mm for successive scallops. Both of these are larger than the depth of cut of a_e=0.004 mm, meaning that successive grinding passes are creating the scallops. According to the *Scallop Waviness Model*, these multiple scallops should be visible. They are not discernable in Figure 10. Therefore, a profile was taken in the grinding direction, shown in Figure 15a.

Here the can see multiple scallops that appear to be carved out by the wheel. If we superimpose on the same distorted scale the profile of a wheel just above the profile, with a_e=0.004 mm as shown in red, we can see that the wheel shape lines up well with the measured profile.

If we put the grinding parameters and wheel run-out into the *Scallop Waviness Model*, we can then choose "random" wave shifts of successive passes with a little care (l_{sh}/l_{wv}= 0.3, 0.75, 0.15, 0.9 and 0.95), we can see how the final profile (Figure 15b, in grey) can closely match the actual profile.

The scallop model was built based on the run-out of a dressed and highly eccentric wheel of RO=2ε=0.081 mm. However, the actual test was performed with a run-out somewhere between the run-out of the dressed wheel and the run-out of the worn wheel (RO=2ε=0.024 mm). It is interesting to note, however, that when the model is built around RO=2ε=0.024 mm, the height of the scallops changes little, from h_{sc}=0.036 mm to h_{sc}=0.028 mm for zero phase shift and from h_{sc}=0.021 mm to h_{sc}=0.020 for the series of random phase shifts given above.

This illustrates that the eccentricity plays a role in the final scallop height, but that the ratio of arc length to chatter wavelength is even more important. Therefore, creep-feed grinding operations with their long arc length and small chatter wavelength are less susceptible to waviness, as demonstrated in Section 4.4, and that cylindrical-grinding operations, with their small effective diameter and larger values of v_w, are particularly susceptible to waviness even when run-out is low.

Figure 15: Measured scallop profile (a) and simulated scallop profile from Scallop-Waviness Model (b).

The *Scallop Waviness Model* can also be used to assess forces. If we put the grinding parameters for the eccentric wheels in Figures 6 and 7 into the model, we obtain a contact time of t_{cont}=36% for Figure 6 and a contact time of 78% for Figure 7. The actual measured contact times were t_{cont}=42% and t_{cont}≈100%, respectively. Therefore, the measured values agree quite well with predicted values, particularly when considering multiple passes were taken with random phase shifts between passes. However, it is interesting to note that, even if the contact time is different, the increase in forces is not affected greatly.

5.2 *Practical Considerations*

Part of the danger with wheel run-out is that operators do not know when it is present. During a recent visit to a European tool manufacturer using state-of-the-art machines, it was seen that the company's standard procedure was to 1) true the diamond wheel on a truing station; 2) remove the wheel from the shaft; 3) mount the wheel on the grinding machine; 4) condition the wheel with an abrasive stick; 5) grind. The company was informed that this is not standard procedure, and that removing the wheel from the shaft – i.e., not using a tapered adaptor – was introducing eccentricity into the wheel that would adversely affect grinding performance. The company claimed the wheel was manufactured to such tight tolerances – H6 – that run-out was minimal. After much pestering, the company agreed to a quick test, and measured run-out after truing and again after carefully dismounting the wheel and remounting it on the truing station. After truing, run-out was 3 μm; after remounting, it had increased to 35 μm.

The company was battling temperature-induced cracking and inconsistent wheel life. The cracking was most likely due to power surges causing higher temperatures coupled with force shocks. The inconsistent wheel life may be due to how "lucky" they were during wheel remounting in obtaining a low eccentricity.

However, as has been shown here, process monitoring can now show issues with wheel eccentricity. Oscillation of force measurements at the wheel frequency can easily pick out wheel run-out, as shown in Figures 6 and 7. Peaks in the FFT from the accelerometer at the wheel speed and harmonics thereof, absent during idling, easily show wheel run-out, as shown in Figure 11. And even a simple method of listening with a microphone can pick out untruth, as shown in Figure 12.

Of course, no wheel is perfectly true, wheels eventually become untrue via collapse [15]. Process monitoring via forces, acceleration and audio would be able to identify this point when dressing is needed. Also, the Scallop Waviness Model can be used to determine when run-out is tolerable and, if so, the necessary wave-shifts in order to obliterate it. This has already been done in cylindrical grinding. In surface grinding, a method could be developed to introduce a predetermined wave-shift in order to reduce the number of spark-out passes required to ensure a small final scallop height. Finally, if eccentricity could be measured, an oscillation of the wheelhead height could be introduced to match this eccentricity, ensuring constant wheel/workpiece contact.

6 CONCLUSIONS

- Grinding forces increase by several times when wheel eccentricity is present, which can result in burn.
- Wheel wear increases with increasing wheel eccentricity.
- Grinding operations with a short wavelength such as creep-feed grinding can show small waviness scallop heights and no evidence of burn but still suffer from higher wheel wear and larger grinding temperatures.
- A simple accelerometer with an FFT can be used to determine if wheel eccentricity is present.
- An audio signal can be used to identify wheel eccentricity.
- All eccentric wheels will experience some attenuation, but critical attenuation where the scallop height is reduced may occur at an arc length lower than the "half wavelength" value that is typically given.
- A model was developed to predict waviness and scallop height from grinding parameters and wheel eccentricity.
- Slightly eccentricity wheels can impart high waviness and very eccentric wheels can impart low waviness depending on the wavelength and the wave-shift.

7 ACKNOWLEDGEMENTS

8 REFERENCES

[1] COLLETCARE. 2009. Spindle Maintenance with Colletcare [Online]. Available from: http://www.precisebits.com/tutorials/coletcareprocedure.htm [Accessed 10/3/2011].

[2] Balancing of Grinding Wheels, Grindwell-Norton/Saint-Gobain brochure.

[3] R. Bennett, C. May, Performance studies on a typical centreless grinding machine with reference to trueing and balancing of the grinding wheel, *Int. J. Mach. Tool Des. Res*, 66 (1965) 47-101.

[4] M. Arizmendi, J. Fernández, L. López de Lacalle, A. Lamikiz, A. Gil, J. Sánchez, F. Campa, F. Feiga, Model development for the prediction of surface topography generated by ball-end mills taking into account the tool parallel axis offset. Experimental Validation. *Annals of CIRP*, 57 (2008) 101-104.

[5] I. Inasaki, B. Karpuschewski, H. Lee, Grinding Chatter – origin and Suppression, *Annals of CIRP*, 5 (2001) 515-534.

[6] E. Armarego, N. Deshpandie, Computerized Predictive Cutting Models of Forces in End-Milling Including Eccentricity Effects, *Annals of CIRP*, 38 (1989) 45-49.

[7] Trmal, G., Holesovsky, F., Wave-shift and its effect on surface quality in super-abrasive grinding, International Journal of Machine Tools & Manufacture, 41, 2001, pp. 979–989.

[8] W. B. Rowe, N. M. Barash, Computer method for investigating the inherent accuracy of centerless grinding, *International Journal of Machine Tool Design and Research*, 4 (1964) 91-116.

[9] W. B. Rowe, Principles of Modern Grinding Technology, William Andrew, 2009.

[10] S. Malkin, C. Guo, Grinding Technology: Theory and Applications of Machining with Abrasives, Second Edition, 2008.

[11] United States Patent US4549372, Sexton *et. al.* 29 October 1985.

[12] J. Badger, Practical Application of Aggressiveness and Chip Thickness in Grinding. J. Badger. *CIRP 3rd International Conference High Performance Cutting (HPC)*, Dublin, Ireland, (2008) 599-606.

[13] J. Badger, 2007, Grindability of Conventionally Produced and Powder-Metallurgy High-Speed Steel, *Annals of CIRP*, 56/1 (2007) 353-356.

[14] J. C. Jaeger, Moving sources of Heat and the Temperature at Sliding Contacts, *Proceedings of the royal society of New South Wales*, 76 (1942) 203-224.

[15] J. Badger, Wheel Collapse in Grinding, *Annals of CIRP*, 58/1 (2009) 307-310.

Highlights

> Grinding-wheel run-out (including eccentricity) leads to scallop-pattern chatter. > Acceleration and noise measurements can be used detect run-out. > Wheel run-out causes force and power surges and increased wheel wear. > Scallop height depends on wheel eccentricity, arc-length and chatter wavelength. > A model was developed to predict chatter scallop height from grinding parameters.
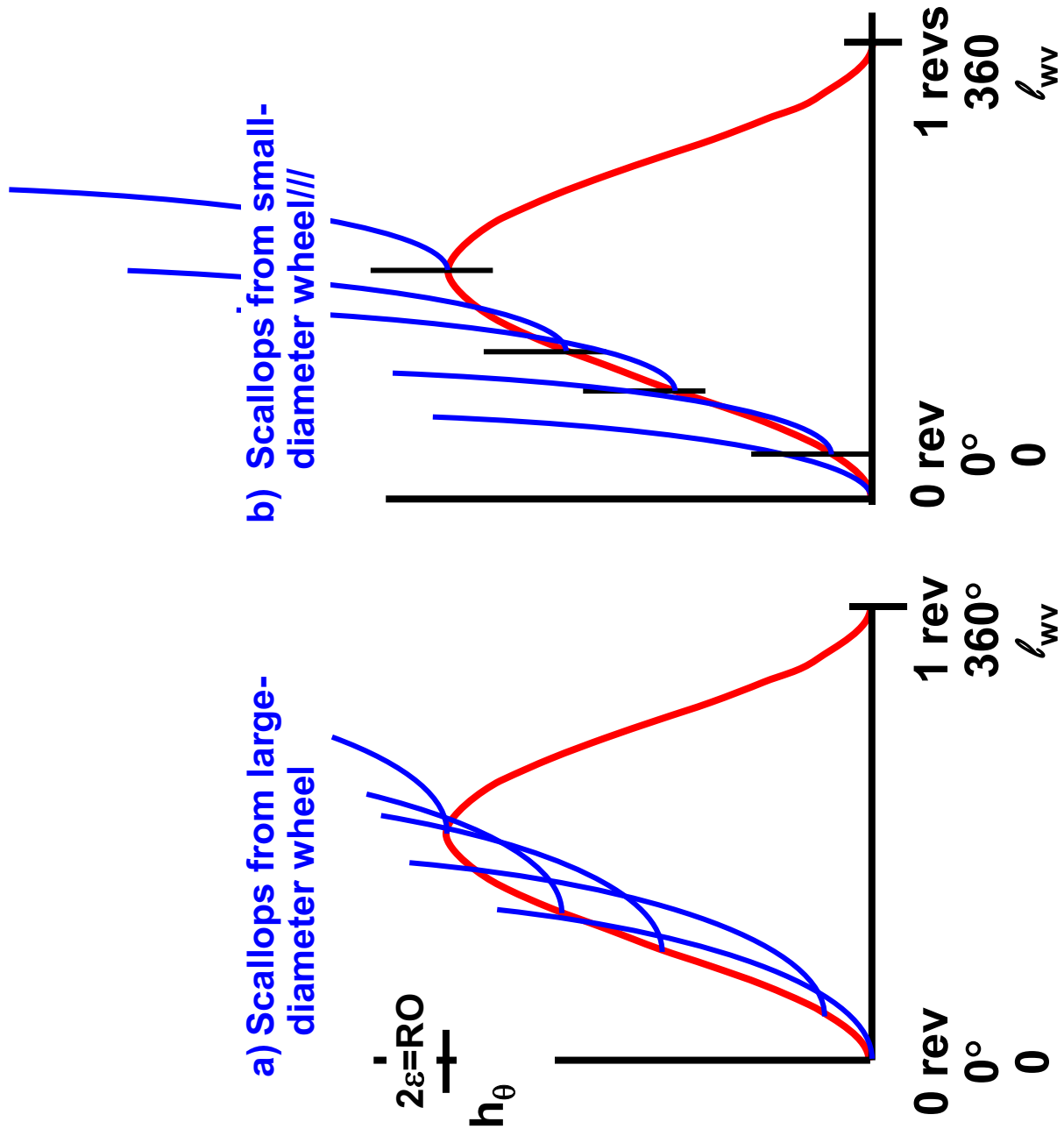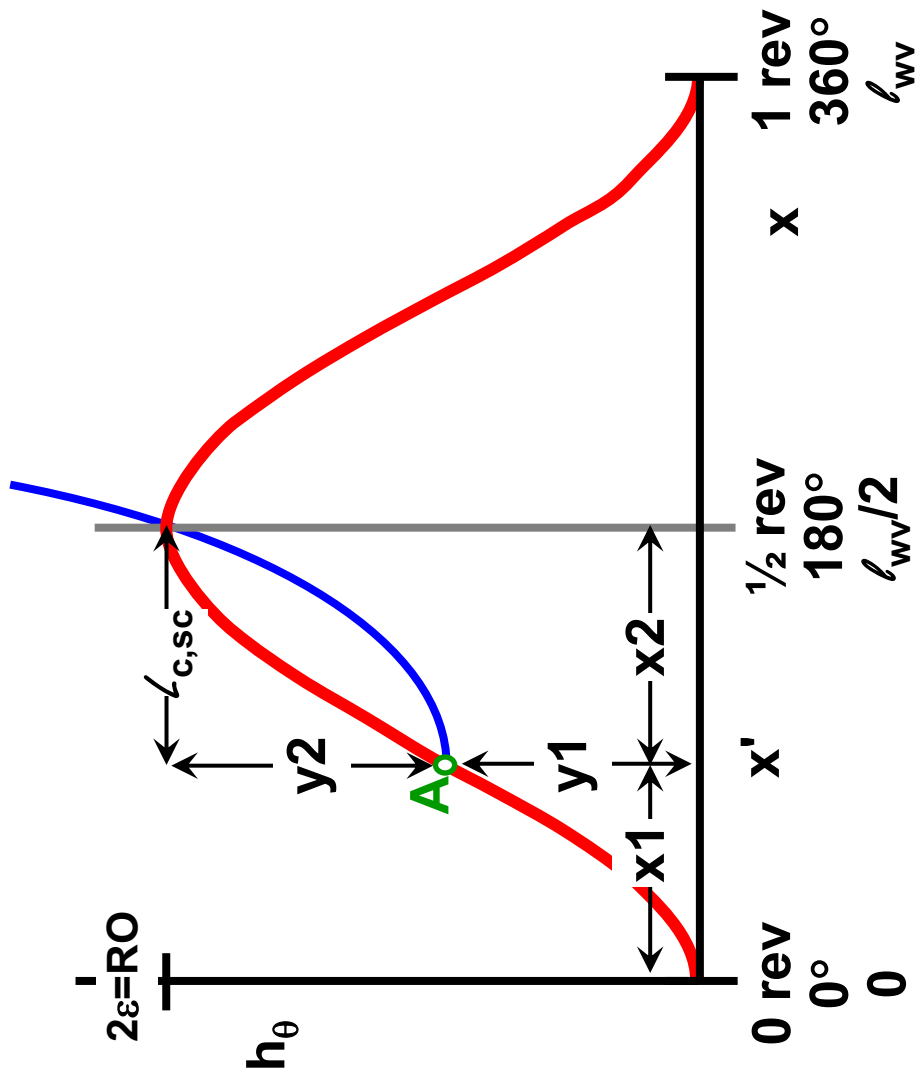
Figures

Figure 1

Figure 2

a) Scallops from large-diameter wheel

b) Scallops from small-diameter wheel///
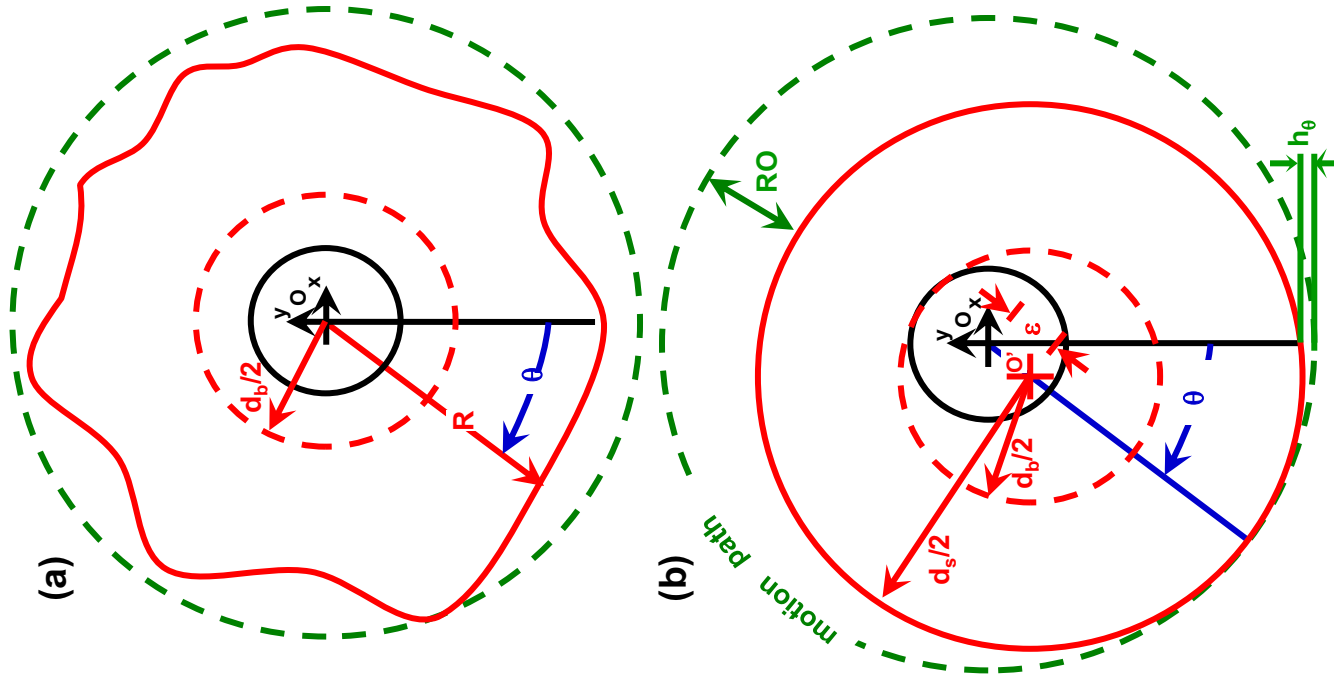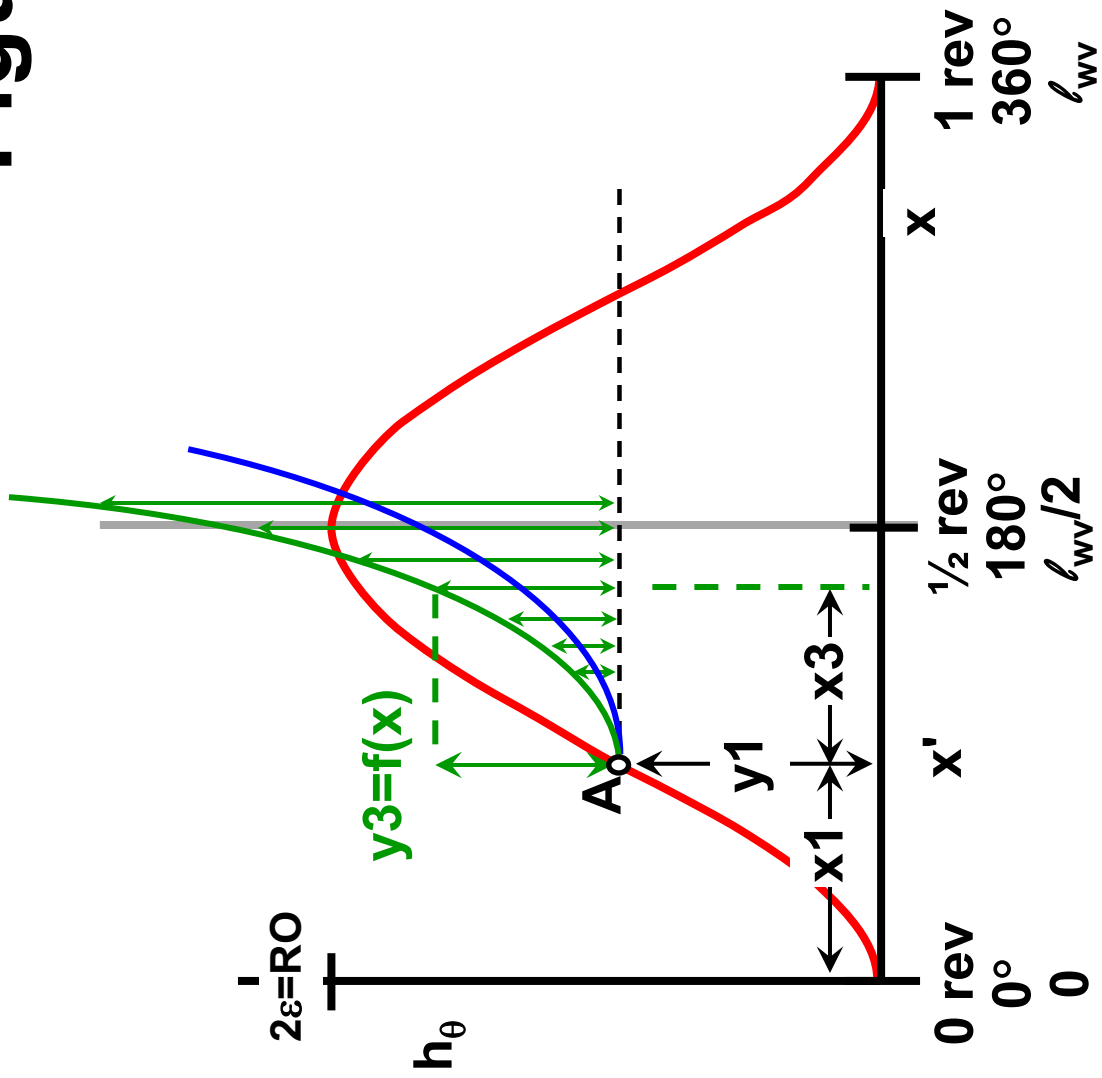
Figure 3

Figure 4

Figure 5
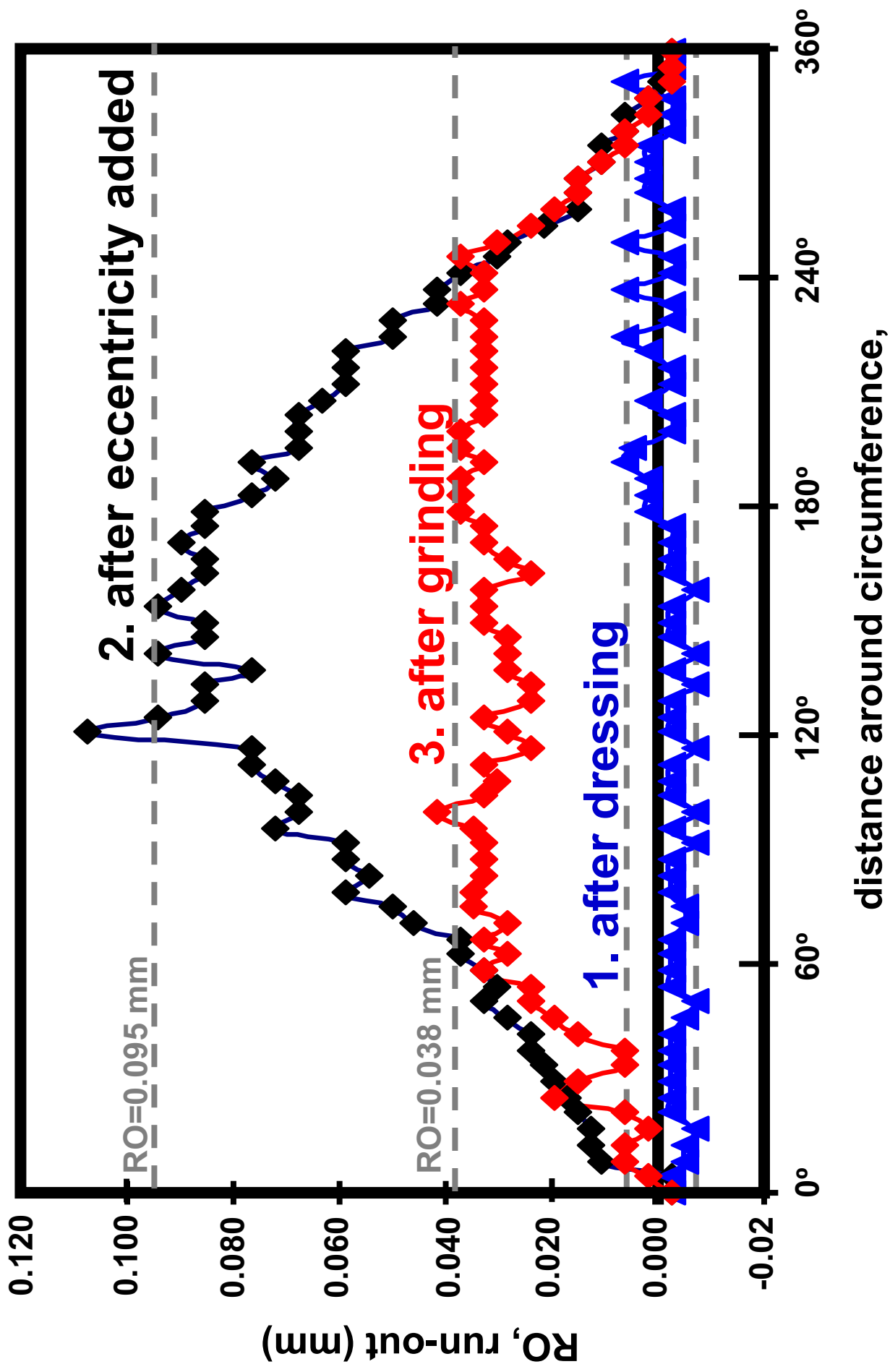
Figure 6
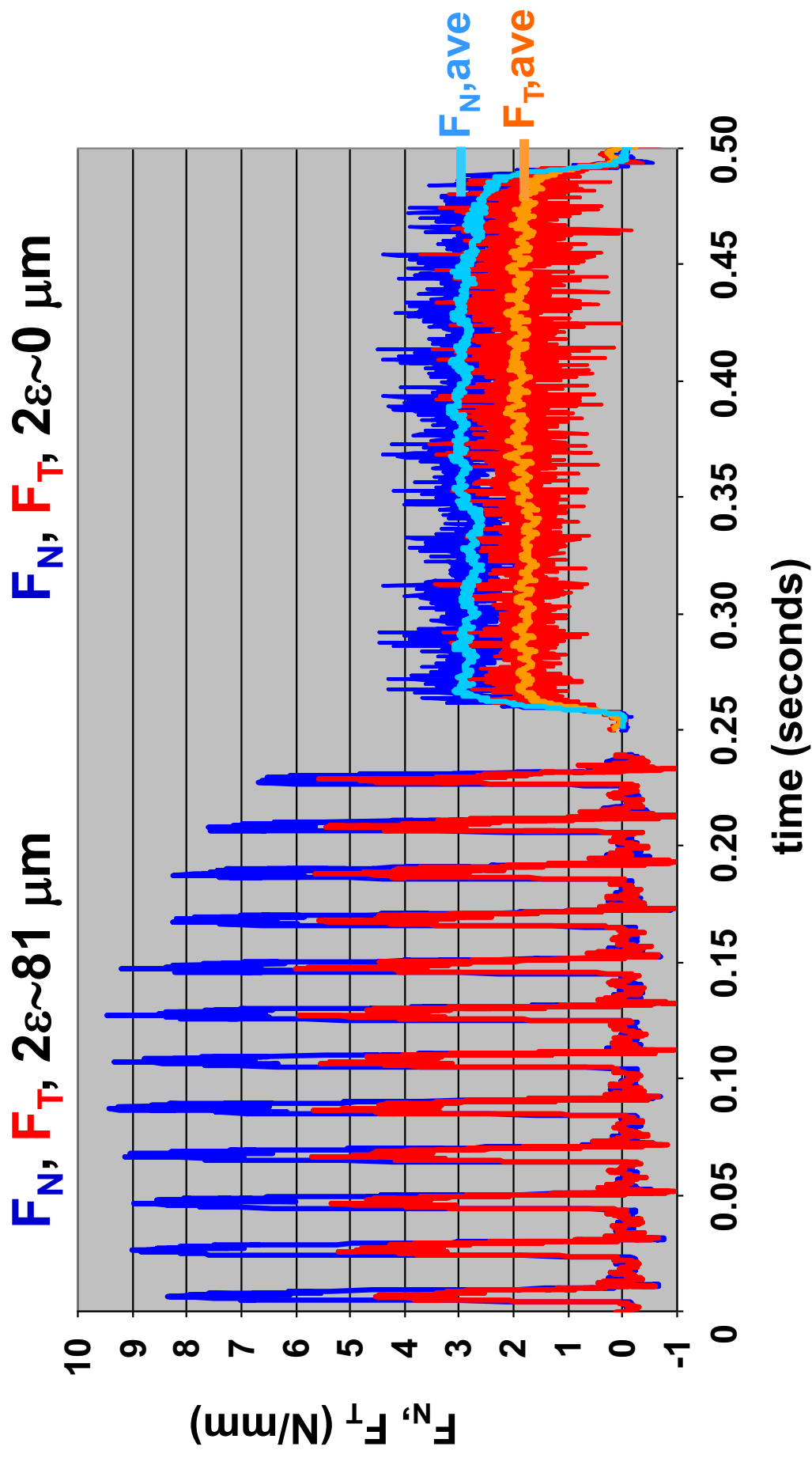
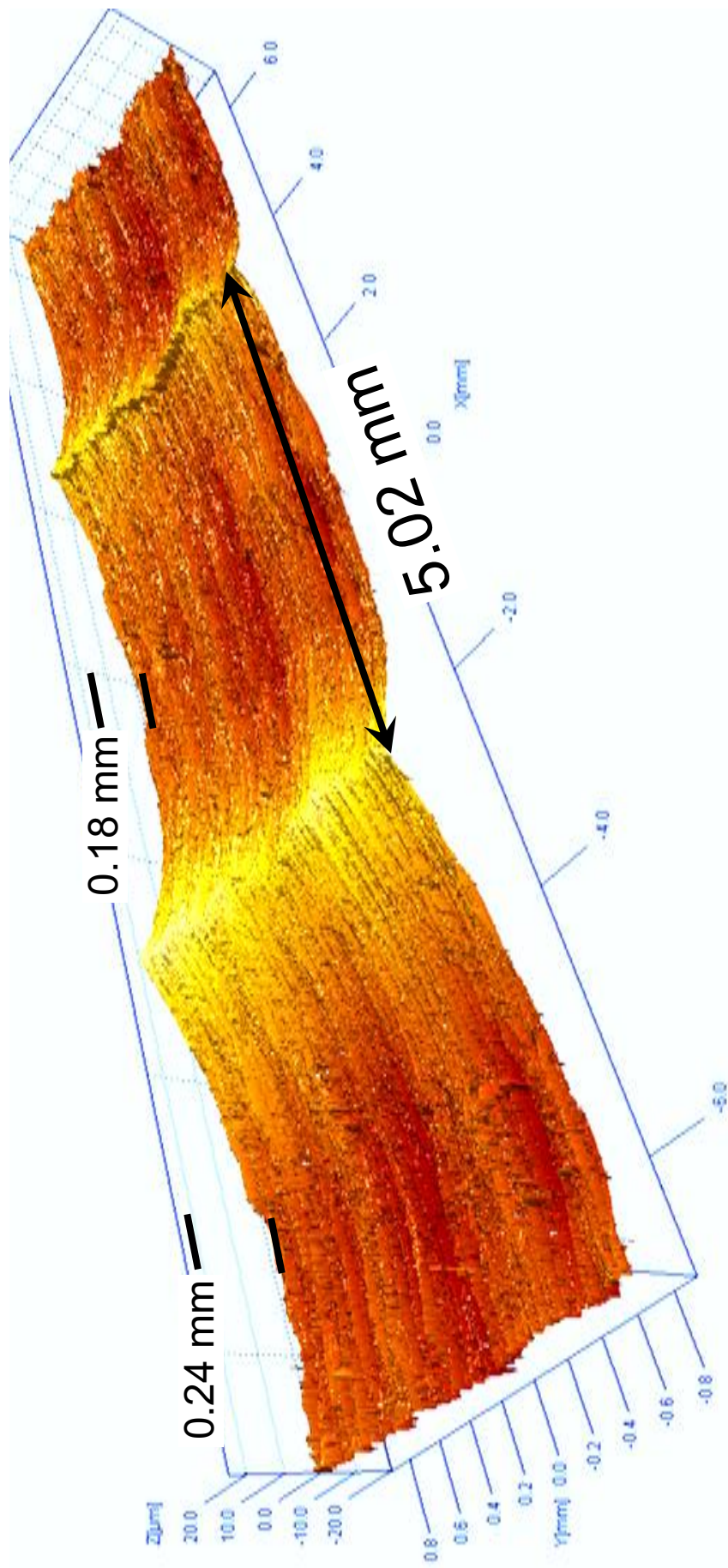Figure 7
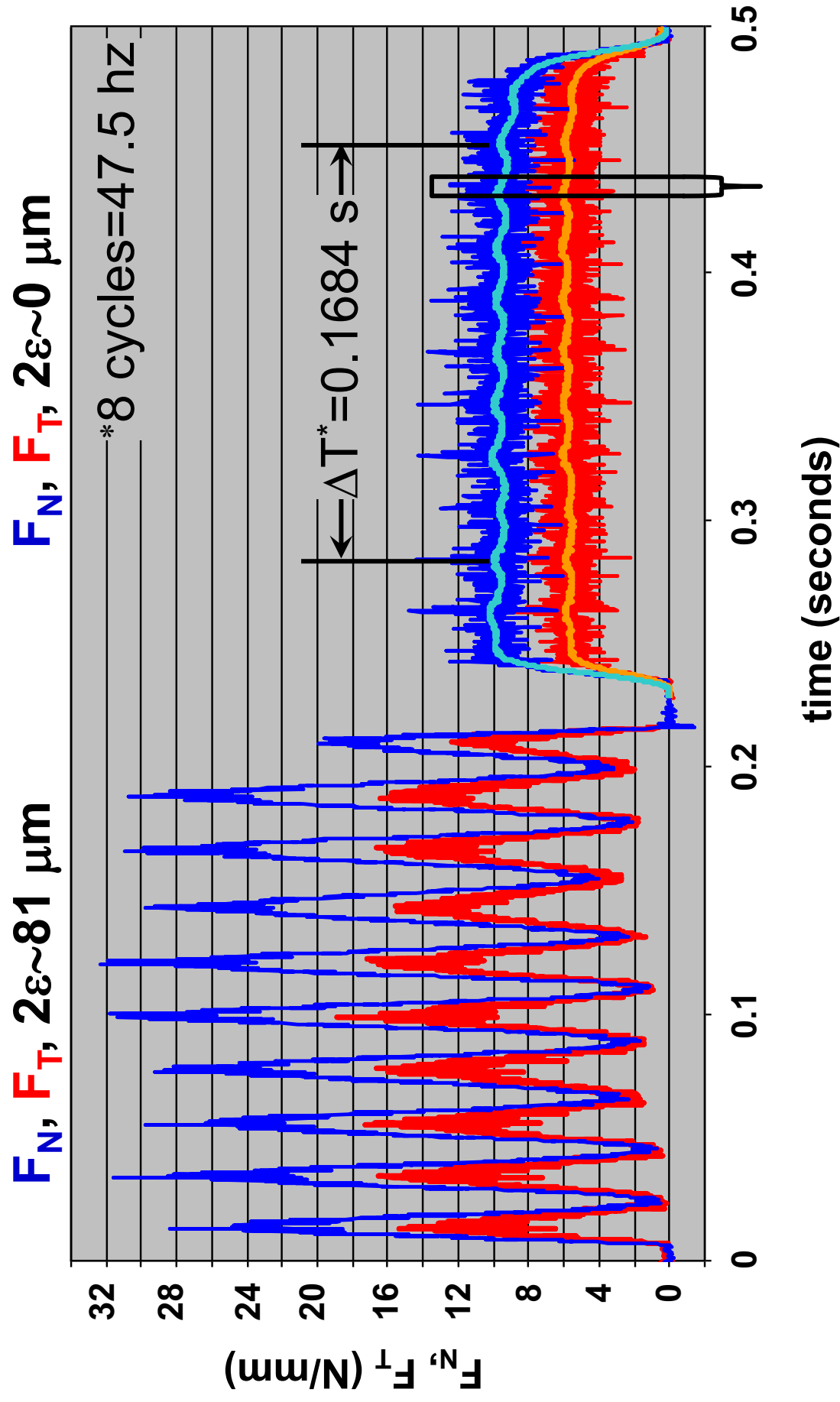
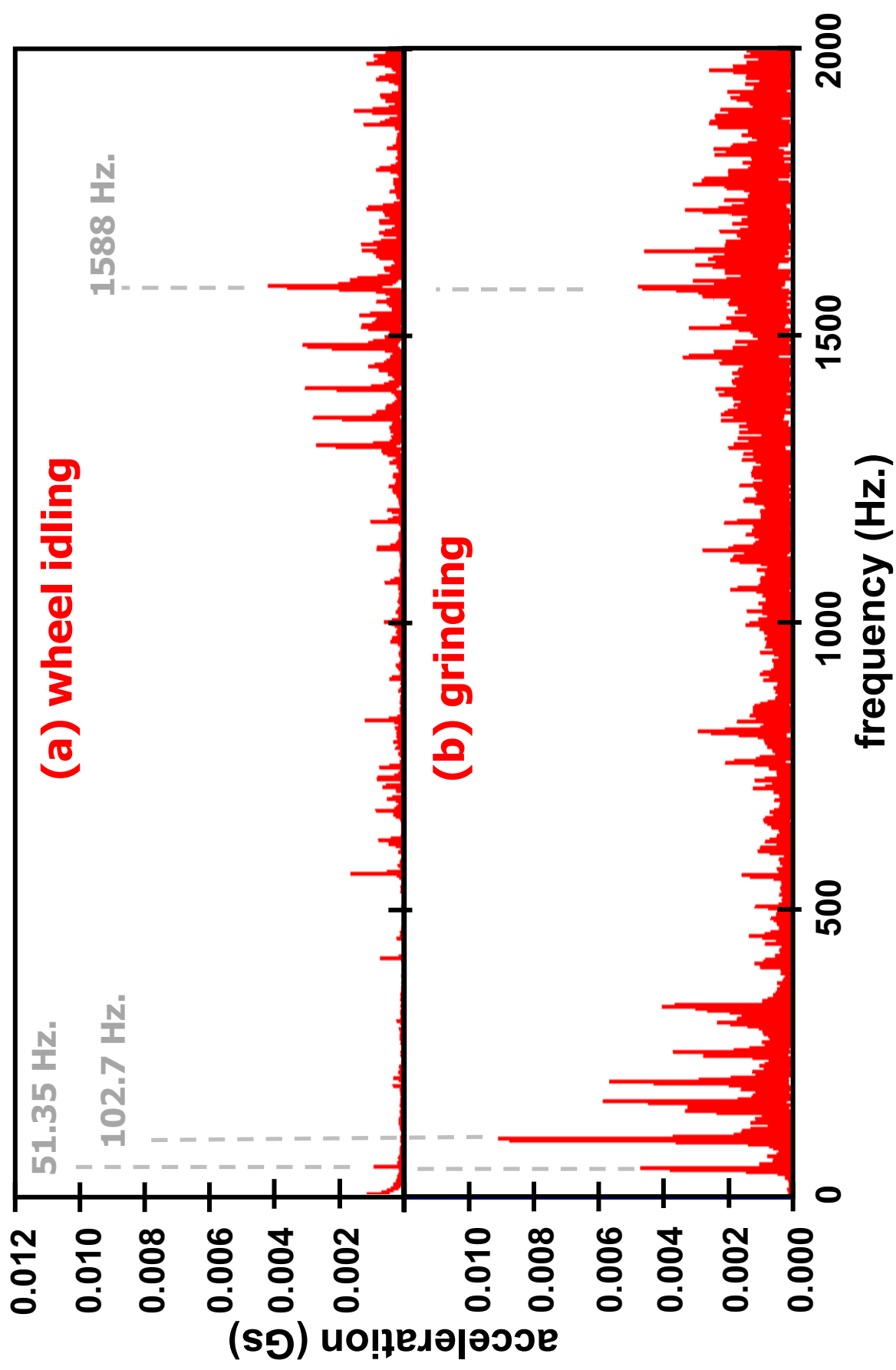# Figure 8
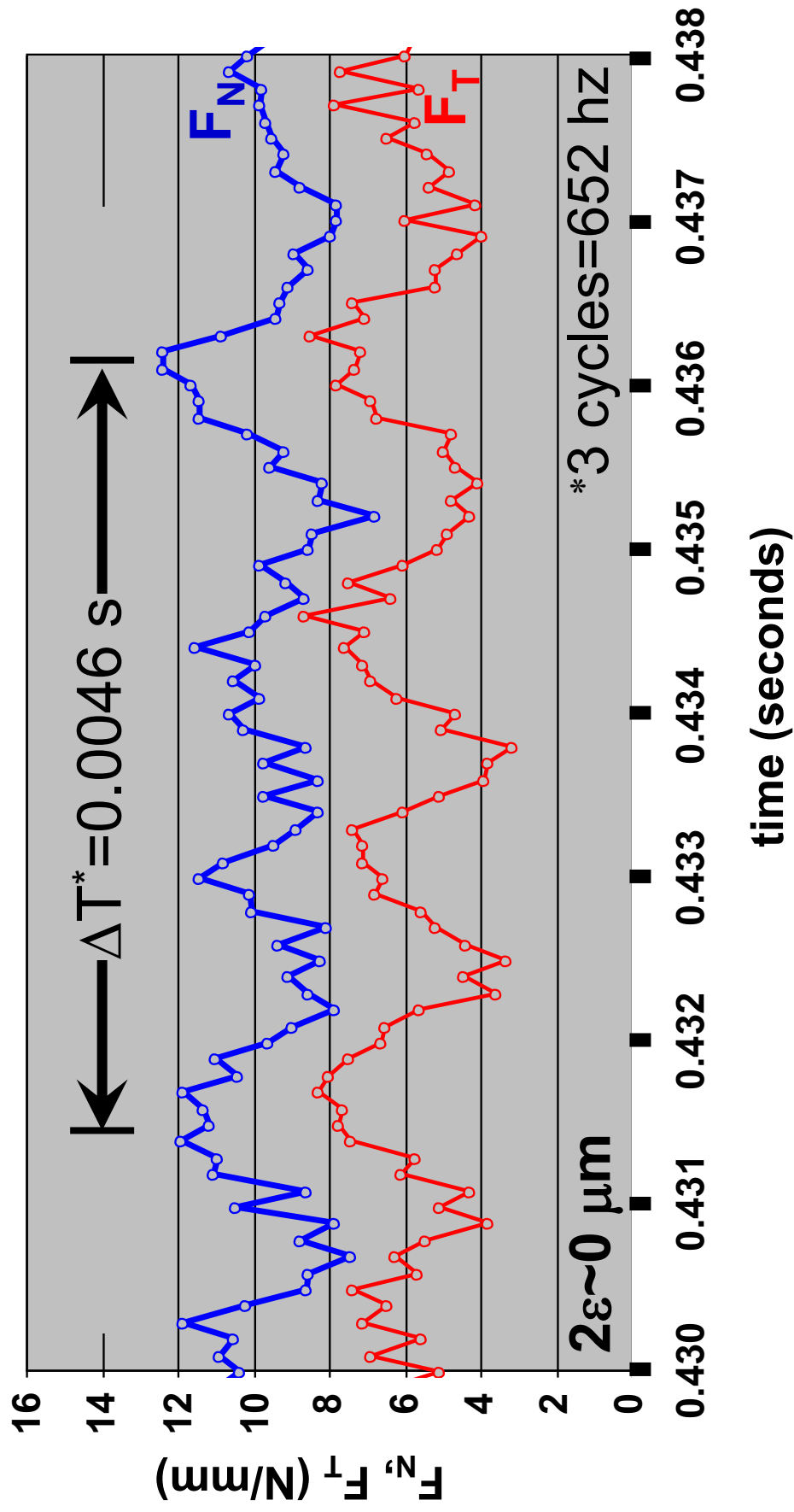
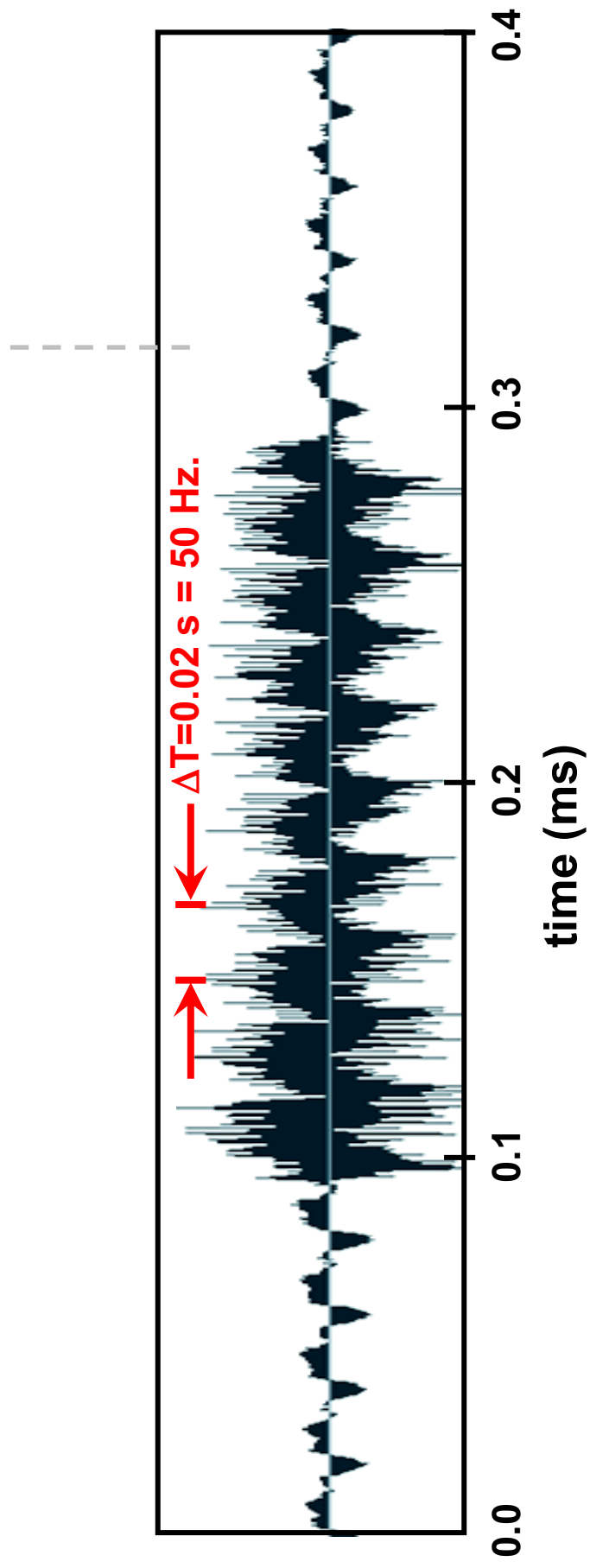# Figure 9

one wheel rev=6.4 mm

Figure 10

Figure 11

Figure 12

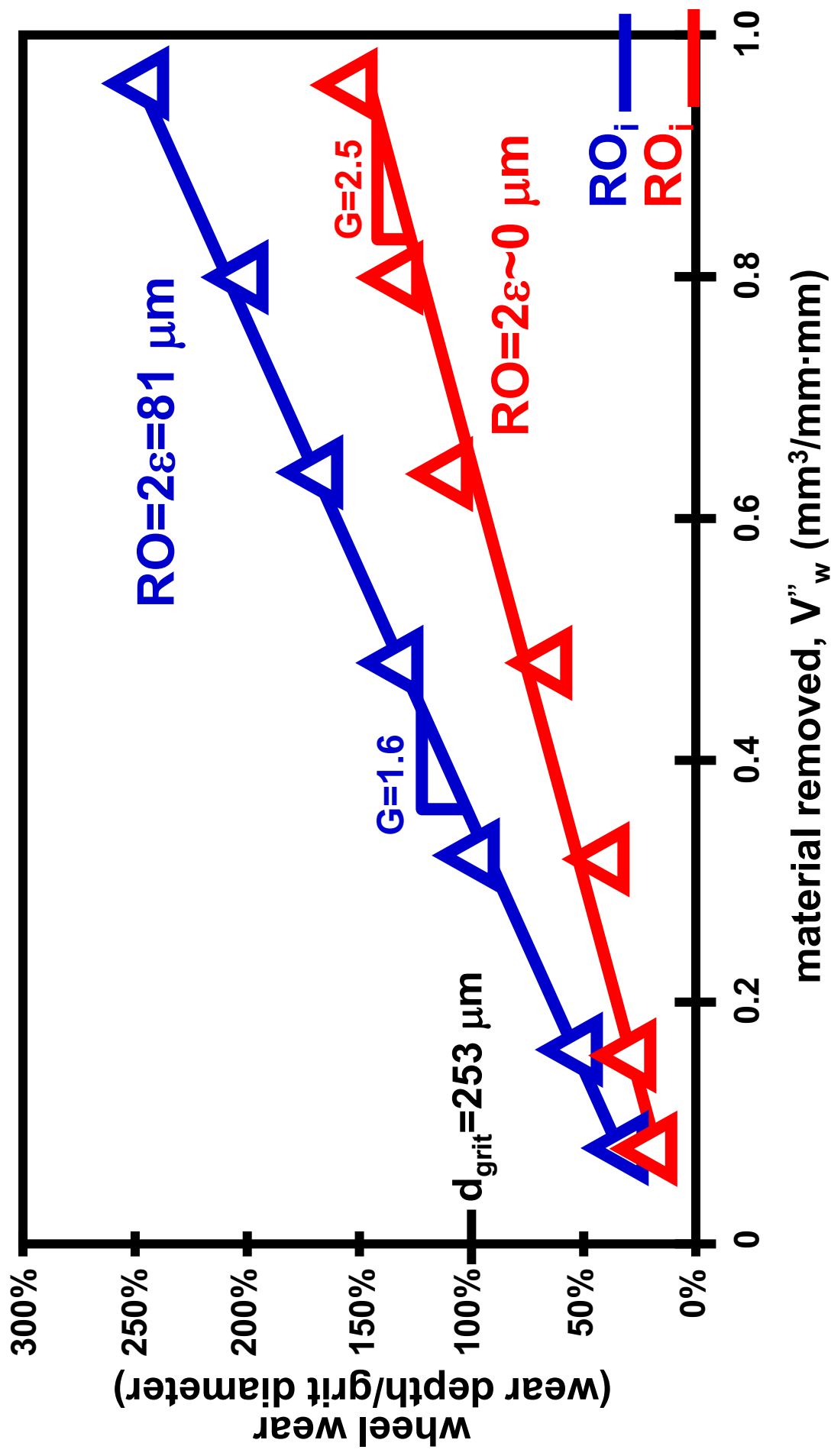ΔT=0.02 s = 50 Hz.

time (ms)

Figure 13

Figure 14

Figure 15

a) Measured scallop profile

b) Scallop profile from scallop-waviness model

Pass 0 Pass 1 Pass 2 Pass 3 Pass 4 Pass 5

height above zero (mm)

distance along workpiece (mm)